Bull. Astr. Soc. India (2004) **32**, 33–57

Transfer of resonance line radiation in advected atmospheres with partial frequency redistribution of photons

A. Peraiah*
57, 4th Cross 36th Main, B T M 1st Stage, Madiwala-Dollar Scheme, Bangalore 560068, India

Received 20 February 2004; accepted 11 March 2004

Abstract. We studied the influence of high velocities of expansion on resonance line radiation by taking into account of aberration and advection. We used an angle averaged redistribution function R_{II} in spherically symmetric media. Three types of media are considered. These are:(1)purely scattering medium (2)partly scattering and emission from continuum medium and (3)partly scattering and continuum and line emission medium. The spherical shells that are being used have thicknesses equal to 2,10 and 100 times the stellar radii. The radiation field is shown in terms of the source functions. Computations are performed in the comoving frame of the gas and the line profiles are calculated at the observer's point at infinity. The line profiles computed in the first type of medium show P Cygni characteristics and those computed in the second and third type of media show central emission and self absorption.

Keywords : radiative transfer - line formation - stellar atmospheres - aberration - advection - redistribution function.

1. Introduction

The outer layers of supergiant stars, novae, supernovae, quasi-stellar objects etc., are expanding with very high velocities. These large velocities introduce two important physical

*e-mail: dspodis@yahoo.com.in

effects, namely aberration and advection (see eq(1) and (2)). The transfer equation contains two types of terms : (1) aberration and advection terms and (2) comoving frame Doppler shift terms. The gas velocity that appears in the aberration and advection terms is measured in units of the velocity of light and that in the comoving frame terms is measured in units of mean thermal units (see eq(9)). We should consider the relative importance of these two types of terms. The velocity terms in the aberration and advection terms are substantially smaller than those in the comoving frame terms. However when the temperature of the medium is high, the mean thermal velocity increases and the number of Doppler units in the comoving frame term reduces while the aberration and advection terms remain constant. Furthermore the quantity m in eq(3) will change considerably when the velocity of the gas increases, making the aberration term very important at high velocities. It was shown earlier (see Peraiah, 1987, 1991a) that even continuum radiation is affected by aberration and advection both in plane parallel and spherically symmetric atmospheres. The effects of high velocities on the formation of resonance lines have been studied in Peraiah(1991b). It was shown that the terms representing aberration advection, namely, $(m+g)\frac{\partial u}{\partial r}$ and $3m^2(\frac{dg}{dr})$ will change the radiation field more than the radial velocity gradient term $m^2\frac{dv}{dr}$. These changes have been shown to be substantial particularly in spherically symmetric atmospheres. The velocity fields produce Doppler shifts and aberration of photons which will lead to advection which describes the "sweeping off" of photons by the moving matter. Spherical symmetry introduces curvature effects and transverse velocity gradients through the terms $\frac{(1-m^2)}{r}\frac{\partial u}{\partial m}$ and $(1-m^2)\frac{v}{r}\frac{\partial u}{\partial x}$ (see eq(1) and (2)). The combined effect of Doppler shifts, curvature, aberration and advection will change the radiation field and the source function. We studied these effects in a resonance line with complete redistribution of photons in Peraiah(1991b). Recently Korčáková and Kubát (2003) studied this problem considering velocities up to 2000 kms^{-1} and concentrated on the effects of aberration only. This study was intended more to examine a new type of solution of the transfer equation than to study the physical effects of aberration and advection on the radiation field.

It is important to study the resonance line radiation using partial frequency redistribution function. We used the angle averaged redistribution function R_{II}, which represents an atom with a perfectly sharp lower state and an upper state broadened by radiative decay. We study the radiation field by computing the source function and the lines at the observer's point. We have considered three physical types of atmospheres.

2. Method of Solution.

The equation of transfer with aberration and advection in the comoving frame is given by,

$$(g+m)\frac{\partial u(r,m,x)}{\partial r}+\frac{1-m^2}{r}\left\{1+mg(1-\frac{r}{g}\frac{dg}{dr})\right\}\frac{\partial u(r,m,x)}{\partial m}$$

$$+3\left\{\frac{g}{r}(1-m^2)+m^2\frac{dv}{dr}\right\}u(r,m,x)-2\frac{(m+g)}{r}u(r,m,x)$$
$$-\left\{\frac{v}{r}(1-m^2)+m^2\frac{dv}{dr}\right\}\frac{\partial u(r,m,x)}{\partial x}=$$
$$K_L(r)[\beta+\phi(r,m,x)][S(r,m,x)-u(r,m,x)], \tag{1}$$

for $0<\mu\leq 1$, and

$$(g-m)\frac{\partial u(r,-m,x)}{\partial r}-\frac{1-m^2}{r}\left\{1-mg(1-\frac{r}{g}\frac{dg}{dr})\right\}\frac{\partial u(r,-m,x)}{\partial m}$$
$$+3\left\{\frac{g}{R}(1-m^2)+m^2\frac{dg}{dr}\right\}u(r,-m,x)-2\frac{(m+g)}{r}u(r,-m,x)$$
$$-\left\{\frac{v}{r}(1-m^2)+m^2\frac{dv}{dr}\right\}\frac{\partial u(r,-m,x)}{\partial x}=$$
$$K_L(r)[\beta+\phi(r,-m,x)][S(r,-m,x)-u(r,-m,x)], attheradialpointr \tag{2}$$

for $-1\leq\mu<0$, where,

$$m=\frac{\mu-g}{1-g\mu}$$
$$g=\frac{v_g}{c} \tag{3}$$

Further, v_g is the gas velocity and c is the velocity of light. We define that $u(r,m,x)=4\pi r^2 I(r,m,x)$, where $I(r,m,x)$ is the specific intensity making an angle $\cos^{-1}\mu$ with the radius vector at the radial point r. K_L is the absorption coefficient at the line centre, ϕ is the line profile function and

$$\beta=\frac{K_c}{K_L} \tag{4}$$

where K_c is the continuum absorption coefficient. The quantity S is the source function and is given by,

$$S(r,m,x)=\frac{\phi(r,m,x)S_L(r,m,x)+\beta S_c(r,x,T_e(r))}{\phi(r,m,x)+\beta} \tag{5}$$

and,

$$S(r,-m,x)=\frac{\phi(r,-m,x)S_L(r,-m,x)+\beta S_c(r,x,T_e(r))}{\phi(r,-m,x)+\beta} \tag{6}$$

Here S_L and S_c are the source functions in the line and continuum respectively. These are given by

$$S_c(r,x,T_e(r))=\rho(r)B(x,T_e(r)), \tag{7}$$

where $B(x, T_e(r))$ is the Planck function at temperature $T_e(r)$ and the normalized frequency x is given by

$$x = \frac{\nu - \nu_0}{\Delta\nu_s} \tag{8}$$

ν and ν_0 being the frequencies in the line and line centre respectively and $\Delta\nu_s$ is a convenient frequency band width normally taken in Doppler units. And $\rho(r)$ is an arbitrary factor normally less than unity. v is the velocity of the gas measured in units of mean thermal velocity. That is,

$$v = \frac{v_g}{v_{therm}} \tag{9}$$

and,

$$v_{therm} = \sqrt{\frac{2kT}{m_{ion}}} \tag{10}$$

where k is the Boltzmann constant, T is the temperature of the gas , m_{ion} is the mass of the ion and v_g is the gas velocity. Further

$$S_L(r, m, x) = \frac{(1-\epsilon)}{2\phi(r, m, x)} \int_{-\infty}^{+\infty} dx' \int_{-1}^{+1} R_{II-A}(x, x') u(r, m', x') dm' + \epsilon B(r, x, T_e(r)) \tag{11}$$

and

$$S_L(r, -m, x) = \frac{(1-\epsilon)}{2\phi(r, -m, x)} \int_{-\infty}^{+\infty} dx' \int_{-1}^{+1} R_{II-A}(x, x') u(r, -m', x') dm' + \epsilon B(r, x, T_e(r)) \tag{12}$$

where ϵ is the probability per scatter that a photon is destroyed by collisional de-excitation. ϕ is the profile function normalised such that

$$\int_{-\infty}^{+\infty} \phi(x) dx = 1 \tag{13}$$

The angle averaged redistribution function $R_{II-A}(x, x')$ is given by,

$$R_{II-A}(x, x') = \pi^{-\frac{3}{2}} \int_{\frac{1}{2}|\bar{x} - \underline{\mathrm{x}}|}^{\infty} e^{-u^2} \left[\tan^{-1} \frac{\underline{\mathrm{x}} + u}{\sigma} - \tan^{-1} \frac{\bar{x} - u}{\sigma} \right] du, \tag{14}$$

where $\bar{x} = \max(|x|, |x|')$, $\underline{\mathrm{x}} = \min(|x|, |x|')$. R_{II-A} was first obtained by Unno (1952). Further,

$$\phi(x) = \int_{-\infty}^{+\infty} R_{II-A(\mathrm{ISO})}(x, x') dx' = H(a, x) \tag{15}$$

We now expand $u(r, m, x)$ as was done in Peraiah(1987). This is given by,

$$u(r,m,x) = u_0 + u_r\xi + u_m\eta + u_x\chi + u_{rm}\xi\eta$$
$$+u_{mx}\eta\chi + u_{xr}\chi\xi + u_{rmx}\xi\eta\chi, \tag{16}$$

where,

$$\xi = \frac{2(r-r')}{\Delta r}, r' = \frac{r_i + r_{i-1}}{2}, \Delta r = r_i - r_{i-1} \tag{17}$$

$$\eta = \frac{2(m-m')}{\Delta m}, m' = \frac{m_j + m_{j-1}}{2}, \Delta m = m_j - m_{j-1} \tag{18}$$

$$\chi = \frac{2(x-x')}{\Delta x}, x' = \frac{x_k - x_{k-1}}{2}, \Delta x = x_k - x_{k-1} \tag{19}$$

We expand the source function in a similar way. Thus,

$$s = s_0 + s_r\xi + s_m\eta + s_x\chi + s_{rm}\xi\eta + s_{mx}\eta\chi$$
$$+s_{xr}\chi\xi + s_{rmx}\xi\eta\chi, \tag{20}$$

where $u_0, ..., u_{rmx}$ and $s_0, ..., s_{rmx}$ are the interpolation coefficients. We have used a discretisation mesh on radius, angle and frequency -(r_i, m_j, x_k). The nodal values of u are

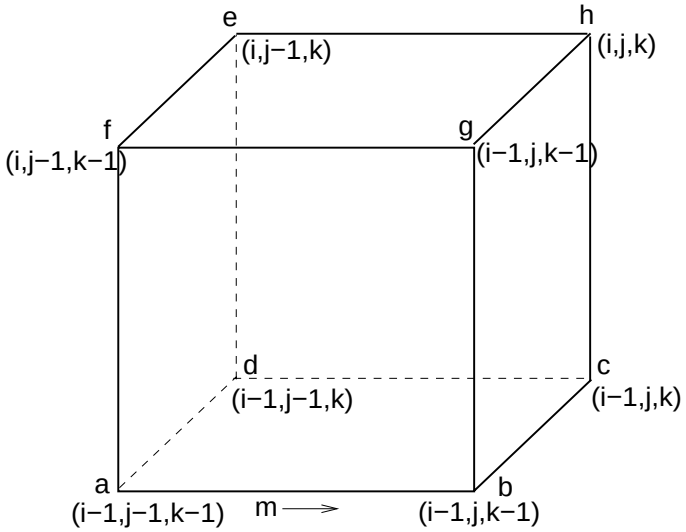

Figure 1. Schematic diagram of angle-radius-frequency grid.

(see Fig.1), $u_a, u_b, u_c, u_d, u_e, u_f, u_g, u_h$. These are obtained in terms of the interpolation coefficients by using equations (16-19). Thus,

$$u_a = u(r_{i-1}, m_{j-1}, x_{k-1}) = u_0 - u_r - u_m - u_x + u_{rm} + u_{mx} + u_{xr} - u_{rmx} \tag{21}$$

$$u_b = u(r_{i-1}, m_j, x_{k-1}) = u_0 - u_r + u_m - u_x - u_{rm} - u_{mx} + u_{xr} + u_{rmx} \tag{22}$$

$$u_c = u(r_{i-1}, m_j, x_k) = u_0 - u_r + u_m + u_x - u_{rm} + u_{mx} - u_{xr} - u_{rmx} \tag{23}$$

$$u_d = u(r_{i-1}, m_{j-1}, x_k) = u_0 - u_r - u_m + u_x + u_{rm} - u_{mx} - u_{xr} + u_{rmx} \tag{24}$$

$$u_e = u(r_i, m_{j-1}, x_k) = u_0 + u_r - u_m + u_x - u_{rm} - u_{mx} + u_{xr} - u_{rmx} \tag{25}$$

$$u_f = u(r_i, m_{j-1}, x_{k-1}) = u_0 + u_r - u_m - u_x - u_{rm} + u_{mx} - u_{xr} + u_{rmx} \tag{26}$$

$$u_g = u(r_i, m_j, x_{k-1}) = u_0 + u_r + u_m - u_x + u_{rm} - u_{mx} - u_{xr} - u_{rmx} \tag{27}$$

$$u_h = u(r_i, m_j, x_k) = u_0 + u_r + u_m + u_x + u_{rm} u_{mx} + u_{xr} + u_{rmx} \tag{28}$$

The interpolation coefficients $u_0, u_r, u_m, etc.$, are obtained from equations (21) to (28) and these are given by,

$$u_0 = \frac{1}{8}(u_a + u_b + u_c + u_d + u_e + u_f + u_g + u_h) \tag{29}$$

$$u_r = \frac{1}{8}(-u_a - u_b - u_c - u_d + u_e + u_f + u_g + u_h) \tag{30}$$

$$u_m = \frac{1}{8}(-u_a + u_b + u_c - u_d - u_e - u_f + u_g + u_h) \tag{31}$$

$$u_x = \frac{1}{8}(-u_a - u_b + u_c + u_d + u_e - u_f - u_g + u_h) \tag{32}$$

$$u_{rm} = \frac{1}{8}(u_a - u_b - u_c + u_d - u_e - u_f + u_g + u_h) \tag{33}$$

$$u_{mx} = \frac{1}{8}(u_a - u_b + u_c - u_d - u_e + u_f - u_g + u_h) \tag{34}$$

$$u_{xr} = \frac{1}{8}(u_a + u_b - u_c - u_d + u_c - u_f - u_g + u_h) \tag{35}$$

$$u_{rmx} = \frac{1}{8}(-u_a + u_b - u_c + u_d - u_e + u_f - u_g + u_h) \tag{36}$$

We substitute equations (16) and (20) into equation (1) and obtain,

$$\begin{aligned}
&\frac{2}{\Delta r}(g+m)(u_r + u_{rm}\eta + u_{xr}\chi + u_{rmx}\eta\chi) \\
&+\frac{2}{\Delta m}(\frac{1-m^2}{r})\left\{1 + mg(1 - \frac{r}{g}\frac{dg}{dr})\right\}(u_m + u_{rm}\xi + u_{mx}\chi + u_{rmx}\xi\chi) \\
&+[3\left\{\frac{g}{r}(1-m^2) + m^2\frac{dg}{dr} + m^2\frac{dg}{dr}\right\} - \frac{2}{r}(m+g)](u_0 + u_r\xi + u_m\eta + \\
&u_x\chi + u_{rm}\xi\eta + u_{mx}\eta\chi + u_{xr}\chi\xi + u_{rmx}\xi\eta\chi) - \frac{2}{\Delta x}\left\{\frac{v}{r}(1-m^2) + m^2\frac{dv}{dr}\right\} \\
&(u_x + u_{mx}\eta + u_{xr}\xi + u_{rmx}\xi\eta) = K_L[\beta' + \phi(r,m,x)][(s_0 + S_r\xi + S_m\eta + S_x\chi \\
&+S_{rm}\xi\eta + S_{mx}\eta\chi + S_{xr}\chi\xi + S_{rmx}\xi\eta\chi) - (u_0 + u_r\xi + u_m\eta + u_x\chi + u_{rm}\xi\eta + \\
&u_{mx}\eta\chi + u_{xr}\chi\xi + u_{rmx}\xi\eta\chi)]
\end{aligned} \tag{37}$$

Similarly equation(2) becomes,

$$\begin{aligned}
&\frac{2}{\Delta r}(g-m)(u_r + u_{rm}\eta + u_{xr}\chi + u_{rmx}\eta\chi) - \frac{2}{\Delta m}(\frac{1-m^2}{r}) \\
&\left\{1 - mg(1 - \frac{r}{g}\frac{dg}{dr})\right\}(u_m + u_{rm}\xi + u_{mx}\chi + urmx\xi\chi) \\
&-\frac{2}{\Delta x}\left\{\frac{v}{r}(1-m^2) + m^2\frac{dv}{dr}\right\}(u_x + u_{mx}\eta + u_{xr}\xi + u_{rmx}\xi\eta) \\
&+[3\left\{\frac{g}{r}(1-m^2) + m^2\frac{dv}{dr}\right\} - \frac{2}{r}(g-m)](u_0 + u_r\xi + u_m\eta + u_x\chi \\
&+u_{rm}\xi\eta + u_{mx}\eta\chi + u_{xr}\chi\xi + u_{rmx}\xi\eta\chi) = K_L[\beta' + \phi(r,-m,x)] \\
&[(S_0 + S_r\xi + S_m\eta + S_x\chi + S_{rm}\xi\eta + S_{mx}\eta\chi + S_{xr}\chi\xi + S_{rmx}\xi\eta\chi) - \\
&(u_0 + u_r\xi + u_m\eta + u_x\chi + u_{rm}\xi\eta + u_{mx}\eta\chi + u_{xr}\chi\xi + u_{rmx})]
\end{aligned} \tag{38}$$

We will now apply the following operators on equations (37) and(38),

$$X_m = \frac{1}{\Delta m}\int_{\Delta m} ...dm, Y_V = \frac{1}{V}\int_{\Delta r} ...4\pi r^2 dr, Z_x = \frac{1}{\Delta x}\int_{\Delta x} ...dx \tag{39}$$

and obtain after a tedious algebra, the following two equations corresponding to equations (1) and (2) respectively. (See Peraiah, 1987). Thus we have,

$$\alpha u_r + \beta' u_m + \gamma u_{rm} + \delta u_0 = \Delta r K_x[S_0 + \frac{1}{6}A_1 S_r]$$
$$+\rho u_x + \sigma u_{xr} + \epsilon' u_{mx} + \lambda u_{rmx}, \tag{40}$$

$$\alpha' u_r + \beta_1 u_m + \gamma' u_{rm} + \delta' u_0 = \Delta r K_x[S_0 + \frac{1}{6}A_1 S_r]$$
$$+\rho u_x + \sigma u_{xr} + \epsilon' u_{mx} + \lambda u_{rmx}, \tag{41}$$

where,

$$A_1' = \frac{\Delta A}{A'}, A' = \frac{V}{\Delta r}, \Delta A = 4\pi(r^2 - r_{i-1}^2), \tag{42}$$

$$V = \frac{4}{3}(r_i^3 - r_{i-1}^3), A_2' = \frac{\Delta A}{V}. \tag{43}$$

We define,

$$g_1 = \frac{dg}{dr}, g_2 = \frac{g_1}{G}, v_d = \frac{dv(r)}{dr}, \tag{44}$$

$$p = \frac{(2 - r' A_2')}{\Delta r}, R = 1 - r g_2, m_2 = (m')^2 + (\frac{\Delta m}{12})^2, \tag{45}$$

$$< m^2 >= \frac{1}{2}(m_j^2 + m_{j-1}^2), G' = \frac{2m'}{\Delta m}(1 - < m^2 >)g, \tag{46}$$

$$\bar{m} = \frac{1 - m_2}{\Delta m}, m_3 = \frac{1}{3m'}, m_4 = \frac{1}{3}\frac{\Delta m}{\Delta r}, \tag{47}$$

$$m_5 = 3m_2 g_1, m_6 = m_3 - g, m_7 = 3m_2 - 1, \tag{48}$$

$$\alpha = \Delta r \left\{ \frac{2}{\Delta r}(m' + g) + \frac{1}{6}A_1' K_x - P[2m' + g(3m_2 - 1)] \right\}$$
$$+\frac{\Delta r}{2} A_1 m_2 g_1, \tag{49}$$

$$\beta' = \Delta r \{A_2'\bar{m} - m'\Delta m[(g+m_3)A_2' - g_1]\}$$
$$+\Delta r G'(\frac{1}{2}A_2' - g_2), \tag{50}$$

$$\gamma = \Delta r(m_4 + Pg' - \frac{1}{6}A_1'G'g_2 + 2P\bar{m} - \Delta m m' m_6 P - \frac{1}{6}A_1'g_1), \tag{51}$$

$$\delta = \Delta r[K_x - \frac{1}{2}A_2'(2m' + gm_7) + 3m_2 g_1], \tag{52}$$

$$\rho = 2\frac{\Delta r}{\Delta x}[\frac{1}{2}A_2'(1-m_2)v_r + m_2 v_d], \tag{53}$$

$$\sigma = 2\frac{\Delta r}{\Delta x}[p(1-m_2)v_r + \frac{1}{6}A_1' m_2 v_d], \tag{54}$$

$$\epsilon' = 2\frac{\Delta r}{\Delta x}[\frac{1}{2}m'\Delta m(v_d - \frac{1}{2}A_2' v_r)], \tag{55}$$

$$\lambda = 2\frac{\Delta r}{\Delta x}[\frac{1}{6}m'\Delta m v_d A_1' - p v_r], \tag{56}$$

$$\alpha' = \Delta r[\frac{2}{\Delta r}(g - m') + \frac{1}{6}A_1' K_x + A_2], \tag{57}$$

$$\beta_1 = \Delta r(B_1 + A_3), \tag{58}$$

$$\gamma' = \Delta r(A_4 + B_2 - m_4), \tag{59}$$

$$\delta' = \Delta r(K_x + A_1), \tag{60}$$

where,

$$A_1 = \frac{1}{2}(2m' = gm_7 + m_5), \tag{61}$$

$$A_2 = p(2m' - gm_7 + \frac{1}{2}m_2 g_1 A_1'), \tag{62}$$

$$A_3 = m'\Delta m[g_1 + \frac{1}{2}A_2'(m_3 - g)], \tag{63}$$

$$A_4 = m'\Delta m[\frac{1}{6}A_1' g_1 + p(m_3 - g)], \tag{64}$$

$$B_1 = \frac{1}{2}A_2' G' - G' g_2 - A_2' \bar{m}, \tag{65}$$

$$B_2 = G' p - \frac{1}{6}A_1' G' g_2 - 2p\bar{m}. \tag{66}$$

We will replace the quantities $u_0, u_r, u_m, ..etc$ in equations (21) to (36) by the nodal values $u_a, u_b, ...etc$ and rewrite equations (37) and(38) as,

$$\begin{aligned} &A_a u_a^+ + A_b u_b^+ + A_c u_c^+ + A_d u_d^+ + A_e u_e^+ + A_f u_f^+ + A_g u_g^+ + A_h u_h^+ \\ &= \tau_x^- (S_a^+ + S_b^+ + S_c^+ + S_d^+) + \tau_x^+ (S_e^+ + S_f^+ + S_g^+ + S_h^+), \end{aligned} \tag{67}$$

$$\begin{aligned} &A_a' u_a^- + A_b' u_b^- + A_c' u_c^- + A_d' u_d^- + A_e' u_e^- + A_f' u_f^- + A_g' u_g^- + A_h' u_h^- \\ &= \tau_x^- (S_a^- + S_b^- + S_c^- + S_d^-) + \tau_x^+ (S_e^- + S_f^- + S_g^- + S_h^-), \end{aligned} \tag{68}$$

where

$$A_a = -\alpha - \beta' + \gamma + \delta + \rho - \sigma - \epsilon' + \lambda, \tag{69}$$

$$A_b = -\alpha + \beta' - \gamma + \delta + \rho - \sigma + \epsilon' - \lambda, \tag{70}$$

$$A_c = -\alpha + \beta' - \gamma + \delta - \rho + \sigma - \epsilon' + \lambda, \tag{71}$$

$$A_d = -\alpha - \beta' + \gamma + \delta - \rho + \sigma + \epsilon' - \lambda, \tag{72}$$

$$A_e = \alpha - \beta' - \gamma + \delta - \rho - \sigma + \epsilon' + \lambda, \tag{73}$$

$$A_f = \alpha - \beta' - \gamma + \delta + \rho + \sigma - \epsilon' - \lambda, \tag{74}$$

$$A_g = \alpha + \beta' + \gamma + \delta + \rho + \sigma + \epsilon' + \lambda, \tag{75}$$

$$A_h = \alpha + \beta' + \gamma + \delta - \rho - \sigma - \epsilon' - \lambda, \tag{76}$$

$$A_a' = -\alpha' - \beta_1 + \gamma' + \delta' + \rho - \sigma - \epsilon' + \lambda, \tag{77}$$

$$A_b' = -\alpha' + \beta_1 - \gamma' + \delta' + \rho - \sigma + \epsilon' - \lambda, \tag{78}$$

$$A'_c = -\alpha' + \beta_1 - \gamma' + \delta' - \rho + \sigma - \epsilon' + \lambda, \tag{79}$$

$$A'_d = -\alpha' - \beta_1 + \gamma' + \delta' - \rho + \sigma + \epsilon' - \lambda, \tag{80}$$

$$A'_e = -\alpha' - \beta_1 - \gamma' + \delta' + \rho + \sigma - \epsilon' + \lambda, \tag{81}$$

$$A'_f = \alpha' - \beta_1 - \gamma' + \delta' + \rho + \epsilon'\sigma - -\lambda, \tag{82}$$

$$A'_g = \alpha' + \beta_1 + \gamma' + \delta' + \rho + \sigma + \epsilon' + \lambda, \tag{83}$$

$$A'_h = \alpha' + \beta_1 + \gamma' + \delta' - \rho - \sigma - \epsilon' - \lambda, \tag{84}$$

$$\tau_x = [\beta + \phi(x)] K_L \Delta r \tag{85}$$

$$\tau_x^+ = \tau_x (1 + \frac{1}{6} A_1) \tag{86}$$

$$\tau_x^- = \tau_x (1 - \frac{1}{6} A_1) \tag{87}$$

The quantities $u_a^+, u_b^+, etc.$, and $u_a^-, u_b^-, etc.$, represent the beams of radiation in the mutually opposite directions (see Figure 1). We make the following substitutions,

$$u_a^+ = u_{j-1,k-1}^{i-1,+}, u_b^+ = u_{j,k-1}^{i-1,+}, u_c^+ = u_{j,k}^{i-1,+}, u_d^+ = u_{j-1,k}^{i-1,+} \tag{88}$$

$$u_e^+ = u_{j-1,k}^{i,+}, u_f^+ = u_{j-1,k-1}^{i,+}, u_g^+ = u_{j,k-1}^{i,+}, u_h^+ = u_{j,k}^{i,+} \tag{89}$$

together with similar equations for $u_a^-, u_b^-, etc.$, and $S_a^+, S_b^+, etc.$, into equations (67) and (68) and obtain equations for $(j-1)^{th}$ and j^{th} angles,given by,

$$\begin{aligned}
&A_{j-1}^a u_{j-1,k-1}^{i-1,+} + A_j^b u_{j,k-1}^{i-1,+} + A_j^c u_{j,k}^{i-1,+} + A_{j-1}^d u_{j-1,k}^{i-1,+} + \\
&A_{j-1}^e u_{j-1,k}^{i,+} + A_{j-1}^f u_{j-1,k-1}^{i,+} + A_j^g u_{j,k-1}^{i,+} + A_j^h u_{j,k}^{i,+} = \tau^- [\\
&\sigma_1 \sum_{k'=-K}^{+K} \sum_{j'=1}^{J} R_{j-1,j'}^{k-1,k'} a_{k'} c_{j'} (u_{j,k-1}^{i-1,+} + u_{j',k-1}^{i-1,-}) + (\epsilon \phi_{k-1}^{j-1} + \rho' \beta) B_{j-1,k-1}^{i-1,+} \\
&+\sigma_1 \sum_{k'=-K}^{K} \sum_{j'=1}^{J} R_{j,j'}^{k-1,k'} a'_k c'_j (u_{j',k-1}^{i-1,+} + u_{j',k-1}^{i-1,-}) + (\epsilon \phi_{k-1}^{j} + \rho' \beta) B_{j,k-1}^{i-1,+}
\end{aligned}$$

$$+\sigma_1 \sum_{k'=-K}^{K} \sum_{j'=1}^{J} R^{k,k'}_{j-1,j'} a'_k c'_j (u^{i-1,+}_{j',k} + u^{i-1,-}_{j',k}) + (\epsilon\phi^j_k + \rho'\beta) B^{i-1,+}_{j,k}$$

$$+\sigma_1 \sum_{k'=K}^{K} \sum_{j'=1}^{J} R^{k,k'}_{j-1,j'} a_k / c'_j (u^{i-1,+}_{j,k} + u^{i-1,-}_{j',k}) + (\epsilon\phi^{j-1}_{k-1} + \rho'\beta) B^{i-1,+}_{j-1,k}]$$

$$+\tau^+ [\sigma_1 \sum_{k'=-K}^{K} \sum_{j'=1}^{J} R^{k,k'}_{j-1,j'} a'_k c'_j (u^{i,+}_{j',k} + u^{i,-}_{j',k}) + (\epsilon\phi^{j-1}_k + \rho'\beta) B^{i,+}_{j-1,k}$$

$$+\sigma_1 \sum_{k'=-K}^{K} \sum_{j'=1}^{J} R^{k-1,k'}_{j,j'} a'_k c'_j (u^{i,+}_{j',k-1} + u^{i,-}_{j',k-1}) + (\epsilon\phi^j_{k-1} + \rho'\beta) B^{i,+}_{j,k-1}$$

$$+\sigma_1 \sum_{k'=-K}^{K} \sum_{j'=1}^{J} R^{k-1,k'}_{j-1,j'} a'_k c'_j (u^{i,+}_{j',k-1} + u^{i,-}_{j',k-1}) + (\epsilon\phi^{j-1}_{k-1} + \rho'\beta) B^{i,+}_{j-1,k-1}$$

$$+\sigma_1 \sum_{k'=-K}^{K} \sum_{j'=1}^{J} R^{k,k'}_{j,j'} a'_k c'_j (u^{i,+}_{j',k} + u^{i,-}_{j',k}) + (\epsilon\phi^j_k + \rho'\beta) b^{i,+}_{j,k}] \tag{90}$$

where $\sigma_1 = \frac{1}{2}(1-\epsilon)$ and i,j and k are the running indices of radial,angle and frequency discretisations respectively. J and $(2K+1)$ are the total number of angles and frequencies respectively. ρ' is an arbitrary parameter usually less than unity. Equation (68) can be written similarly. These two equations can be rewritten for J angles as,

$$(A^{ab} u^{i-1,+}_{k-1} - \tau^- \sigma_1 Q Y^{i-1,+}_{k-1}) + (A^{dc} u^{i-1,+}_k - \tau^- \sigma_1 Q Y^{i-1,+}_k)$$
$$+(A^{fg} u^{i,+}_{k-1} - \tau^+ \sigma_1 Q Y^{i,+}_{k-1}) + (A^{eh} u^{i,+}_k - \tau^+ \sigma_1 Q Y^{i,+}_k) =$$
$$\tau^- \sigma_1 Q (Y^{i-1,+}_{k-1} + Y^{i-1,-}_k) + \tau^+ \sigma_1 Q (Y^{i,-}_{k-1} + Y^{i,-}_k) + \tau^- \sigma_1 Q (\rho'\beta + \epsilon\phi_{k-1}) B^{i-1}_{k-1} +$$
$$\tau^- \sigma_1 Q (\rho'\beta + \epsilon\phi_k) B^{i-1}_k + \tau^+ \sigma_1 Q (\rho'\beta + \epsilon\phi_{k-1}) B^i_{k-1}$$
$$+\tau^+ \sigma_1 Q (\rho'\beta + \epsilon\phi_k) B^i_k \tag{91}$$

and,

$$(D^{ab} u^{i-1,-}_{k-1} - \tau^- \sigma_1 Q Y^{i-1,-}_{k-1}) + (D^{dc} u^{i-1,-}_{k-1} - \tau^- \sigma_1 Q Y^{i-1,-}_k) +$$
$$(D^{fg} u^{i,-}_{k-1} - \tau^+ \sigma_1 Q Y^{i,-}_{k-1}) + (D^{eh} u^{i,-}_k - \tau^+ \sigma_1 Q Y^{i,-}_k) =$$
$$\tau^- \sigma_1 Q (\rho'\beta + \epsilon\phi_{k-1}) B^{i-1}_{k-1} + \tau^- \sigma_1 Q (\rho'\beta + \epsilon\phi_k) B^{i-1}_k +$$
$$\tau^+ \sigma_1 Q (\rho'\beta + \epsilon\phi_{k-1}) B^i_{k-1} + \tau^+ \sigma_1 Q (\rho'\beta + \epsilon\phi_k) B^i_k +$$
$$\sigma_1 (\tau^- + \tau^+) Q (Y^{i-1,+}_{k-1} + Y^{i-1,+}_k) \tag{92}$$

where,

$$A^{ab} = \begin{bmatrix} A^a_{j-1} & A^b_j & & & \\ & A^a_j & A^b_{j+1} & & \\ & & \ddots & \ddots & \\ & & & A^a_{J-1} & A^b_J \\ & & & & A^a_J \end{bmatrix} \tag{93}$$

$$D^{ab} = \begin{bmatrix} A^{'a}_{j-1} & A^{'b}_j & & & \\ & A^{'a}_j & A^{'b}_{j+1} & & \\ & & \ddots & \ddots & \\ & & & A^{'a}_{J-1} & A^{'b}_J \\ & & & & A^{'a}_J \end{bmatrix} \tag{94}$$

$$Q = \begin{bmatrix} 1 & 1 & & & \\ & 1 & 1 & & \\ & & \ddots & \ddots & \\ & & & 1 & 1 \\ & & & & 1 \end{bmatrix} \tag{95}$$

For J angles(J rows and J columns)

$$u^{i+1,+}_{k-1} = \begin{bmatrix} u(r_{i-1}, m_{j-1}, x_{k-1}) \\ u(r_{i-1}, m_j, x_{k-1}) \\ \cdots \\ u(r_{i-1}, m_J, x_{k-1}) \end{bmatrix} \tag{96}$$

and,

$$Y^{i-1,+}_{k-1} = R_{k-1} W_k u^{i-1,+}_{k-1} \tag{97}$$

$$W_l = [W_l \delta_{ll'}] \tag{98}$$

$$W_l = a_k c_j, l = j + (k-1)J, 1 \leq l \leq L, L = JK \tag{99}$$

The matrices A^{dc} , A^{fg} , A^{eh} , D^{dc} , D^{fg} , D^{eh} are expressed in a similar manner. WE define the following matrices:

$$\begin{aligned} &(A^{ab}_q, A^{dc}_q, A^{fg}_q, A^{eh}_q, D^{ab}_q, D^{dc}_q, D^{fg}_q, D^{eh}_q) = \\ &Q^{-1}(A^{ab}, A^{dc}, A^{fg}, A^{eh}, D^{ab}, D^{dc}, D^{fg}, D^{eh}) \end{aligned} \tag{100}$$

Equations (91) and (92) can be rewritten as

$$
\begin{aligned}
&(A_q^{ab}u_{k-1}^{i-1,+} - \tau^-\sigma_1 Y_{k-1}^{i-1,+}) + (A_q^{dc}u_k^{i-1,+} - \tau^-\sigma_1 Y_k^{i-1,+}) \\
&+(A_q^{fg}u_{k-1}^{i,+} - \tau^+\sigma_1 Y_{k-1}^{i,+}) + (A_q^{eh}u_k^{i,+} - \tau^+\sigma_1 Y_k^{i,+}) \\
&= \tau^-\sigma_1(Y_{k-1}^{i-1,+} + Y_k^{i-1,+}) + \tau^+\sigma_1(Y_{k-1}^{i,-} + Y_k^{i,-}) + \\
&\tau^-\sigma_1(\rho'\beta + \epsilon\phi_{k-1})B_{k-1}^{i-1} + \tau^-\sigma_1(\rho'\beta + \epsilon\phi_k)B_k^{i-1} + \\
&\tau^+\sigma_1(\rho'\beta + \epsilon\phi_{k-1})B_{k-1}^{i} + \tau^+\sigma_1(\rho'\beta + \epsilon\phi_k)B_k^{i},
\end{aligned} \tag{101}
$$

and,

$$
\begin{aligned}
&(D_q^{ab}u_{k-1}^{i-1,-} + \tau^-\sigma_1 Y_{k-1}^{i-1,-}) + (D_q^{dc}u_k^{i-1,-} - \tau^-\sigma_1 Y_k^{i-1,-}) \\
&+(D_q^{fg}u_{k-1}^{i,-} - \tau^+\sigma_1 Y_{k-1}^{i,-}) + (D_q^{eh}u_k^{i,-} - \tau^+\sigma_1 Y_k^{i,-}) \\
&= \tau^-\sigma_1(Y_{k-1}^{i-1,+} + Y_k^{i-1,+}) + \tau^+\sigma_1(Y_{k-1}^{i,-} + Y_k^{i,-}) + \\
&\tau^+\sigma_1(\rho'\beta + \epsilon\phi_{k-1})B_{k-1}^{i-1} + \tau^-\sigma_1(\rho'\beta + \epsilon\phi_k)B_k^{i-1} + \\
&\tau^-\sigma_1(\rho'\beta + \epsilon\phi_{k-1})B_{k-1}^{i-1} + \tau^+\sigma_1(\rho'\beta + \epsilon\phi_k)B_k^{i}
\end{aligned} \tag{102}
$$

We now write equations (101) and (102) for $K(1 \le k \le K)$ for K frequency points. These ar,

$$
\begin{aligned}
&(\bar{\mathbf{A}}_{dc}^{ab} - \tau^-\sigma_1\mathbf{F}_{i-1}^{++})\mathbf{u}_{i-1}^{+} + (\bar{\mathbf{A}}_{eh}^{fg} - \tau^+\sigma_1\mathbf{F}_i^{++})\mathbf{u}_i^{+} = \\
&\tau^-\sigma_1(\mathbf{F}_{i-1}^{+-}\mathbf{u}_{i-1}^{-} + \mathbf{\Phi}_i\mathbf{B}_i) + \tau^+\sigma_1(\mathbf{F}_i^{+-}\mathbf{u}_i^{-} + \mathbf{\Phi}_i\mathbf{B}_i)
\end{aligned} \tag{103}
$$

and,

$$
\begin{aligned}
&(\bar{\mathbf{D}}_{dc}^{ab} - \tau^-\sigma_1\mathbf{F}_{i-1}^{--})\mathbf{u}_{i-1}^{-} + (\bar{\mathbf{D}}_{eh}^{fg} - \tau^+\sigma_1\mathbf{F}_i^{--})\mathbf{u}_i^{-} = \\
&\tau^-\sigma_1(\mathbf{F}_{i-1}^{-+}\mathbf{u}_{i-1}^{+} + \mathbf{\Phi}_{i-1}\mathbf{B}_{i-1}) + \tau^+\sigma_1(\mathbf{F}_i^{-+}\mathbf{u}_i^{+} + bf\Phi_i\mathbf{B}_i)
\end{aligned} \tag{104}
$$

where,

$$
\bar{\mathbf{A}}_{dc}^{ab} = \mathbf{Q}_F^{-1}\mathbf{A}_{dc}^{ab} \tag{105}
$$

Matrices $\bar{\mathbf{A}}_{eh}^{fg}$,$\bar{\mathbf{D}}_{dc}^{ab}$,$\bar{\mathbf{D}}_{eh}^{fg}$ are similarly defined. And,

$$
\mathbf{Q}_F = \begin{bmatrix}
\mathbf{I} & \mathbf{I} & & & \\
 & \mathbf{I} & \mathbf{I} & & \\
 & & \ddots & \ddots & \\
 & & & \mathbf{I} & \mathbf{I} \\
 & & & & \mathbf{I}
\end{bmatrix} \tag{106}
$$

where $\mathbf{I}$ is the identity matrix. Furthermore,

$$
\mathbf{A}_{dc}^{ab} = \begin{bmatrix}
\mathbf{A}_{q,k-1}^{ab} & \mathbf{A}_{q,k}^{dc} & & & \\
 & \mathbf{A}_{q,k}^{ab} & \mathbf{A}_{q,k+1}^{dc} & & \\
 & & \ddots & \ddots & \\
 & & & \mathbf{A}_{q,K-1}^{ab} & \mathbf{A}_{q,k}^{dc} \\
 & & & & \mathbf{A}_{q,K}^{ab}
\end{bmatrix} \tag{107}
$$

$$\mathbf{F}_i = [\mathbf{RW}]_\mathbf{i} \tag{108}$$

As the redistribution function R is not affected by the motion of the gases in the comoving frame, it remains constant at all the spatial points. This gives us,

$$\mathbf{F} = \mathbf{F}^{++} = \mathbf{F}^{+-} = \mathbf{etc}, . \tag{109}$$

$$\mathbf{\Phi}^i = [\rho'\beta + \epsilon\phi_k^i]\delta_{kk'} \tag{110}$$

$$\mathbf{B}_i = [B_{k,i}]\mathbf{L}, \mathbf{L} = [\mathbf{1_1}, \mathbf{1_2}, ...\mathbf{1_k}, ...\mathbf{1_K}]^\mathbf{T} \tag{111}$$

The matrices $\mathbf{A}_{eh}^{fg}$,$\mathbf{D}_{dc}^{ab}$,$\mathbf{D}_{eh}^{fg}$ are similarly defined. Equations (103) and(104) can be

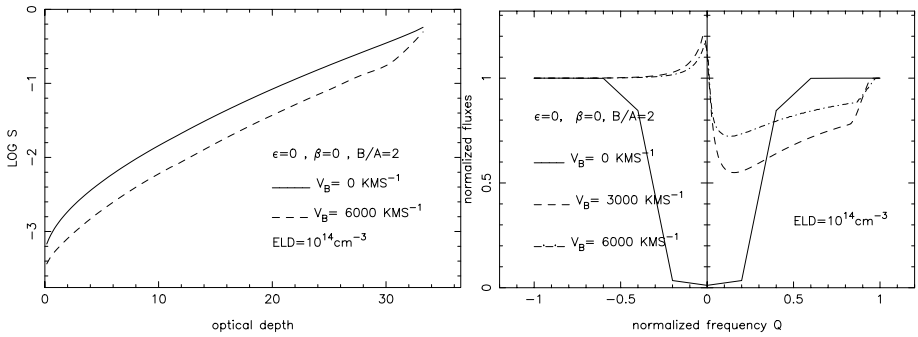

Figure 2. Source functions are given in the left part of the figure and the corresponding line profiles are shown in the right part of the figure.

written in the form of interaction principle(Peraiah,2002) and obtain the transmission and reflection operators $\mathbf{T}(i, i-1)$,$\mathbf{T}(i-1, i)$,$\mathbf{R}(i, i-1)$,$\mathbf{R}(i-1, i)$ and the source vectors $\mathbf{\Sigma}^+$ and $\mathbf{\Sigma}^-$ in the cell. Let us write,

$$\mathbf{F}^+ = \tau^+\sigma_1\mathbf{F}, \mathbf{F} = \tau^-\sigma_\mathbf{1}\mathbf{F} \tag{112}$$

$$\mathbf{G} = \bar{\mathbf{A}}_\mathbf{eh}^\mathbf{fg} - \mathbf{F}^+, \mathbf{H} = \bar{\mathbf{D}}_\mathbf{dc}^\mathbf{ab} - \mathbf{F}^- \tag{113}$$

$$\mathbf{P} = \bar{\mathbf{A}}_\mathbf{dc}^\mathbf{ab} - \mathbf{F}^-, \mathbf{S} = \bar{\mathbf{D}}_\mathbf{eh}^\mathbf{fg} - \mathbf{F}^+ \tag{114}$$

and write the$\mathbf{T}$ and $\mathbf{R}$ operators as follows,

$$\mathbf{T}(i, i-1) = \mathbf{R}^{+-}\mathbf{G}^{-1}[\mathbf{F}^-\mathbf{H}^{-1}\mathbf{F}^- - \mathbf{P}] \tag{115}$$

$$\mathbf{T}(i-1, i) = \mathbf{R}^{-+}\mathbf{H}^{-1}[\mathbf{F}^+\mathbf{G}^{-1}\mathbf{F}^+ - \mathbf{S}] \tag{116}$$

$$\mathbf{R}(i, i-1 = \mathbf{R}^{-+}\mathbf{H^{-1}}[\mathbf{F}^{-} - \mathbf{F}^{+}\mathbf{G^{-1}}\mathbf{P}] \tag{117}$$

$$\mathbf{R}(i-1, i) = \mathbf{R}^{-+}\mathbf{G}^{-1}[\mathbf{F}^{+} - \mathbf{F}^{-}\mathbf{H}^{-1}\mathbf{S}]. \tag{118}$$

The source vectors are,

$$\mathbf{\Sigma}^{+}_{i-\frac{1}{2}} = \sigma_1 \mathbf{R}^{+-}\mathbf{G}^{-1}[(\tau^{-}\mathbf{\Phi}_{i-1}\mathbf{B}_{i-1} + \tau^{+}\mathbf{\Phi}_i\mathbf{B}_i)$$
$$+\mathbf{F}^{-}\mathbf{H}^{-1}(\tau^{-}\mathbf{\Phi}_{i-1}\mathbf{B}_{i-1} + \tau^{+}\mathbf{\Phi}_i\mathbf{B}_i)] \tag{119}$$

$$\mathbf{\Sigma}^{-}_{i-\frac{1}{2}} = \sigma_1 \mathbf{R}^{-+}\mathbf{H}^{-1}[(\tau^{-}\mathbf{\Phi}_{i-1}\mathbf{B}_{i-1} + \tau^{+}\mathbf{\Phi}_i\mathbf{B}_i)$$
$$+\mathbf{F}^{+}\mathbf{G}^{-1}(\tau^{-}\mathbf{\Phi}_{i-1}\mathbf{B}_{i-1} + \tau^{+}\mathbf{\Phi}_i\mathbf{B}_i)] \tag{120}$$

3. Results and Discussion.

We used the transmission and the reflection operators and the source vectors given in eqs(115-120) to compute the internal radiation field (see Peraiah ,2002). We considered spherical atmospheres whose ratios of outer to inner radii(B/A) are 2,10 and 100. The inner radius is always set equal to 10^{12} cm while the outer radii are set equal to 2×10^{12} cm ($B/A = 2$), 10^{13} cm ($B/A = 10$) and 10^{14} cm ($B/A = 100$). We used a velocity law in which the velocity increases with radius and the density changes according to the law of coservation. We used the redistribution function given in eq(14) and a Voigt profile function. The maximum velocities at $r = B$ are taken as $V_B = 0, 3000, 6000$ kms^{-1} while the velocities at $r = A$ are always set equal to $V_A = 0$ kms^{-1}. This implies that we have taken a maximum velocity of expansion equal to 0.02c. We selected

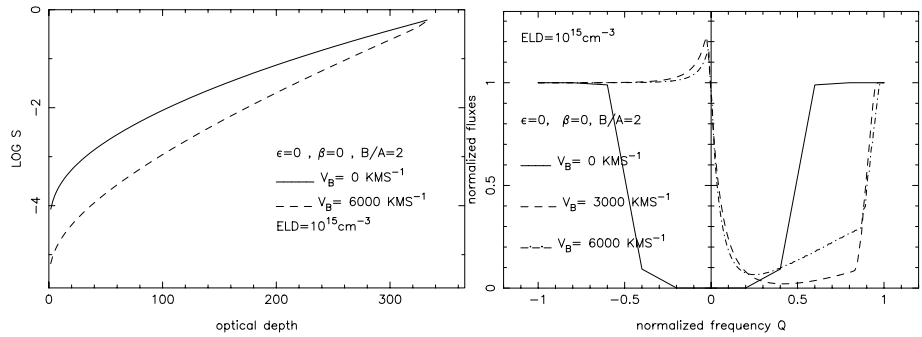

Figure 3. Source functions and corresponding line profiles.

two electron densities ELD for the purpose of computing the optical depths. These are $10^{14} and 10^{15} cm^{-3}$. We used 4 Gaussian points for the angle quadrature on $0 < \mu \leq 1$. These are:$\mu_1 = 0.06943, \mu_2 = 0.33001, \mu_3 = 0.66999, \mu_4 = 0.93057$,and the corresponding

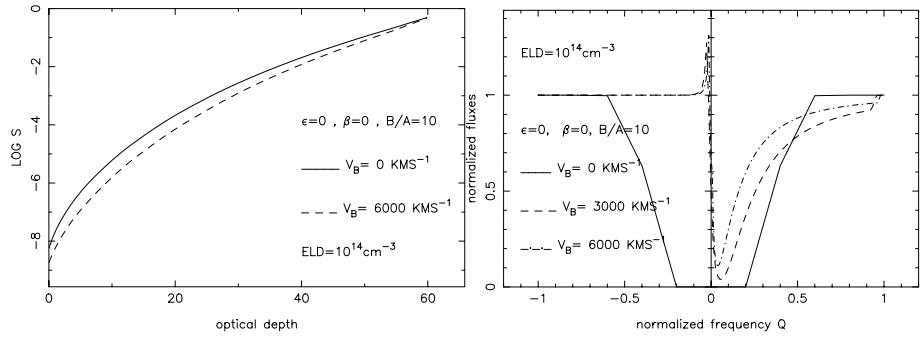

Figure 4. Source functions and corresponding line profiles.

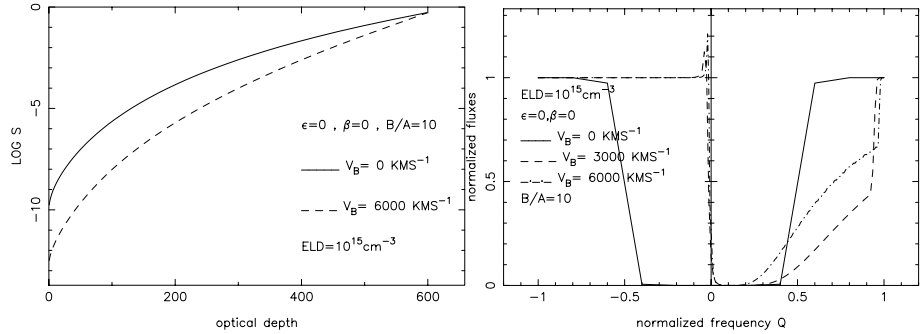

Figure 5. Source functions and the e corresponding line profiles.

weights are $c_1 = 0.17393, c_2 = 0.32607, c_3 = c_2 and c_4 = c_1$. We have chosen trapezoidal points for the frequency grid with the normalized frequency points x_k where

$$x_k = \frac{\nu - \nu_0}{\Delta\nu_D} \tag{121}$$

where $\Delta\nu_D$ is the Doppler width. The radial grid is set by dividing the atmosphere into 100 shells each of equal radial thickness whose optical depths will be increasing in the outward direction. This means that the shell at $r = A$ will be optically thicker than that at $r = B$. We have used the angle averaged redistribution function R_{II} in the scattering integral of the source function(see eq(14)) and a profile function as given in eq(15). A temperature of $100,000K$ is used so that the mean thermal velocity is large enough to have the Doppler units by which the gas velocity is measured, manageably low, while the factor $g(= v/c)$ remains constant irrespective of the temperature of the gas. For a temperature of 10^5K , the mean thermal units (see eq(9)) will be about 148 for hydrogen gas and $g = v/c \approx 0.02$ for $V_B = 6000$ kms^{-1}. The quantity m in eq(3) is a function of the velocity of expansion. For a velocity of 6000 kms^{-1} $m_1 = 0.04955$, 30 per cent less than $\mu_1.m_4$ will differ from μ_4 by few percent. These changes in the cosines of the angles of the rays will produce large effects on the radiation field by introducing aberration and

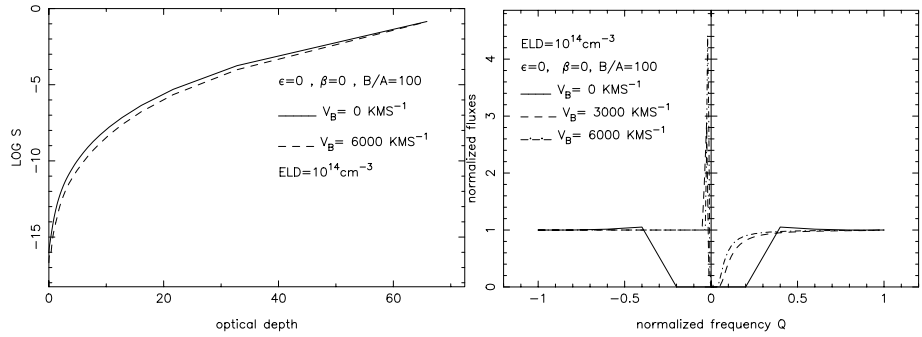

Figure 6. Source functions and the corresponding line profiles.

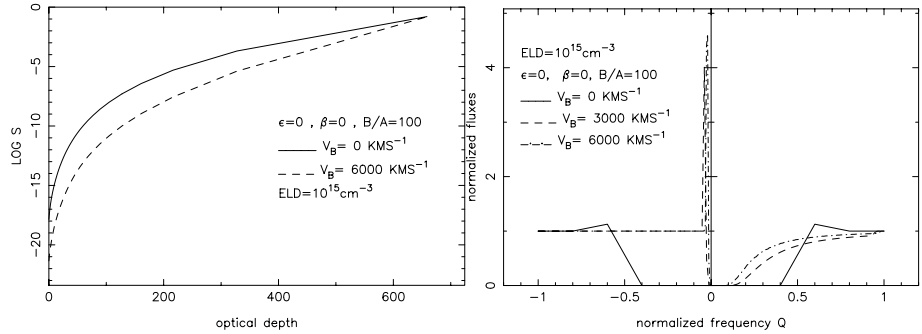

Figure 7. Source functions and the corresponding line profiles.

advection. We considered three types of atmospheres: Case(1)$\epsilon = 0$, $\beta = 0$. This is a purely scattering atmosphere. The boundary conditions for radiation field are:

$$u^-(m_j, \tau = \tau_{max}, x) = 1, \tag{122}$$

and

$$u^+(m_j, \tau = 0, x) = 0. \tag{123}$$

where τ_{max} occurs at $r = A(= 10^{12} cm)$and $\tau = 0$ occurs at$r = B(= 2\times10^{12}, 10^{13}, 10^{14} cm)$. No incident radiation is given from outside. The boundary conditions for velocities are already explained. The results are given in figures (2-7). Case(2): $\epsilon = 10^{-3}$, $\beta = 0$. In this case , the line gets contribution of photons from those scattered and partially redistributed and from those that are thermalised in the continuum. The Plank function contributes to the continuum which is set equal to

$$B(T(r), x) = 1, \tag{124}$$

and the boundary conditions of the radiation field are given by,

$$u^-(m_j, \tau = \tau_{max}, x) = 0, \tag{125}$$

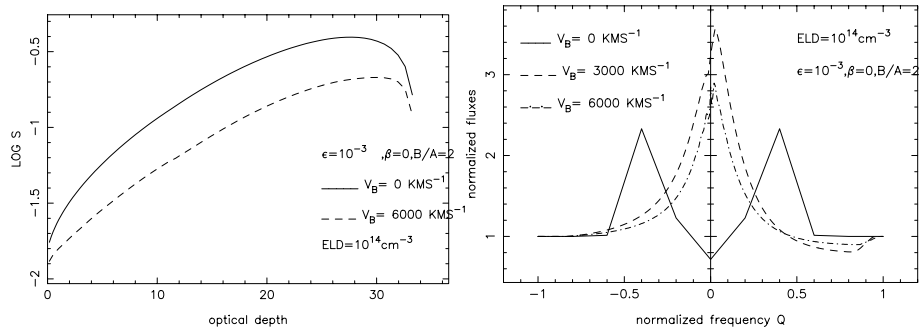

Figure 8. Source functions and the corresponding line profiles.

$$u^+(m_j, \tau = 0, x) = 0. \tag{126}$$

This means that there is no incident radiation on either side of the atmosphere. The

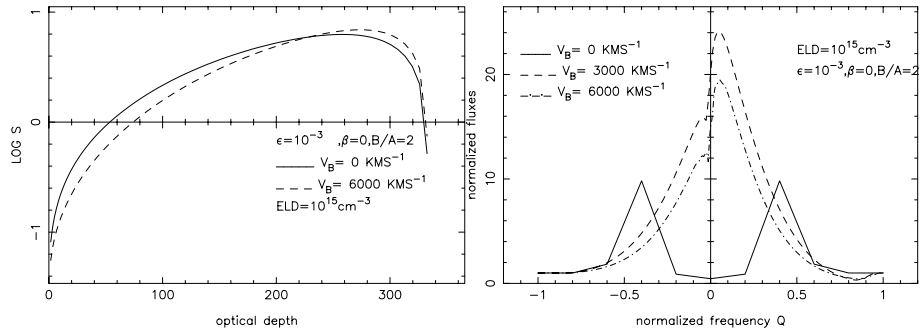

Figure 9. Source functions and the corresponding line profiles.

results are given in figures(8-13). Case(3): $\epsilon = 10^{-3}$, $\beta = 10^{-3}$. This is a case in which the line gets photons from the scattered pool, continuum and from the line emission. The boundary conditions in this case are same as those given in case(2). The factor in eq(7) is set equal to 1. The results of this case are presented in figures(14-19). The calculations are angle-sensitive(m is dependent on the velocity of expansion) and therefore we chose 4 angles on Gauss-Legendre quadrature. The quantities Δr_I,Δm_J,Δx_K are taken to be as follows:

$$\Delta r_I = r_I, \tag{127}$$

$$\Delta m_J = m_J, \tag{128}$$

$$\Delta x_K = x_K. \tag{129}$$

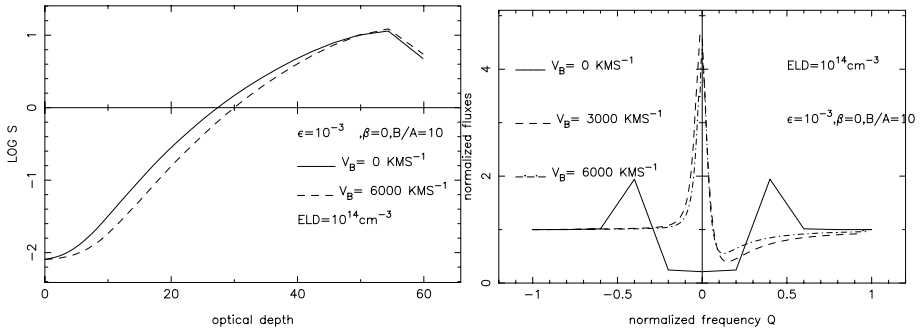

Figure 10. Source functions and the corresponding line profiles.

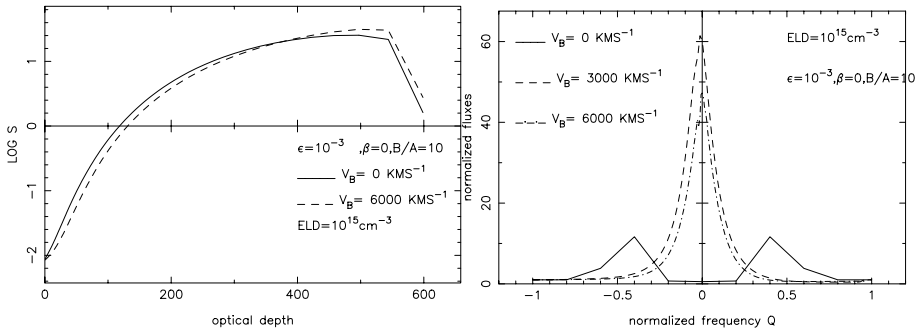

Figure 11. Source functions and the corresponding line profiles.

Similarly we have written $r' = r_I$, $m' = m_J$ and $x' = x_K$. These approximations reduce the accuracy to certain extent but the accuracy can be improved considerably by taking a large sized mesh on angle frequency and radius. The source functions given in eq(5) and the corresponding line profiles are given in each of the figures (2-19). The source functions vary considerably from $\tau = 0$ to $\tau = \tau_{max}$. It is found to be convenient to show the logarithmic values of the source functions instead of their real values. The differences between the source functions in the static medium and those in the expanding media are considerably large and the logarithmic values tend to show as if these differences are small. The line profiles are computed in the observer's frame by using Voigt profile function with a damping constant of 10^{-3}. For details of this computation see Peraiah (2002, chap 8). These profiles show normalised fluxes versus normalised frequencies. These are defined as follows:

$$Q_k = \frac{x_k}{x_{K=-I}} \tag{130}$$

$$F_x = \frac{F_Q(x)}{F_c} \tag{131}$$

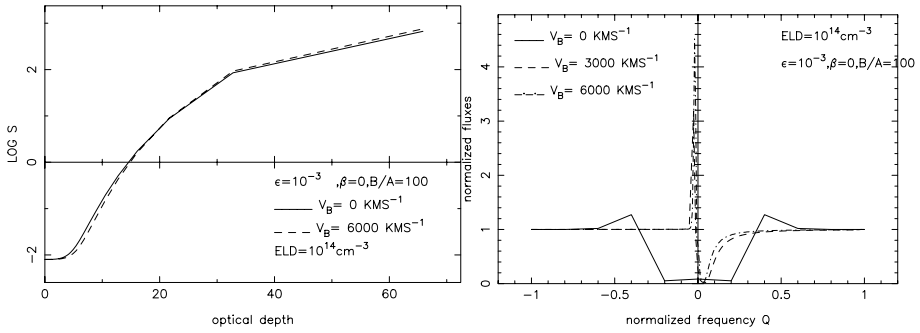

Figure 12. Source functions and the corresponding line profiles.

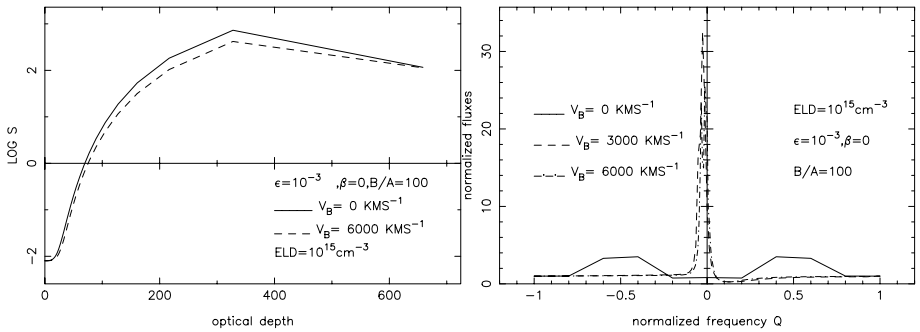

Figure 13. Source functions and the corresponding line profiles.

where $F_c$is the flux in the continuum. Each of the figures contain the relevant information that is used to obtain the results shown in the figure. The part of the figure which contains the source functions give the source functions corresponding to $V_B = 0$ and $V_B = 6000$ kms^{-1} only, while the part of the graph which shows the line profiles shoe curves corresponds to $V_B = 0, V_B = 3000, V_B = 6000$ kms^{-1}. This is done to avoid overcrowding in the source function graphs. It would be interesting to compare the results in atmospheres with different geometrical thicknesses and optical thicknesses. Therefore we used affixed set of the values of B/A and the electron density(ELD). We shall examine how these two parameters change the radiation field when aberration and advection are taken into account. Figures(2-7) contain the results of the first model. The optical depths change from a maximum of 30for $B/A = 2$ with $ELD = 10^{14} cm^{-3}$ to more than 600 for $B/A = 100$ with $ELD = 10^{15} cm^{-3}$. There is no emission of radiation from the medium except the scattered photons which are incident at $\tau = \tau_{max}$ (see the boundary conditions). Therefore the source functions show minima at $\tau = 0$ and maxima at $\tau = \tau_{max}$. For example, the source function in figure 2, for $v_B = 0$ kms^{-1} change by a factor of 6.3×10^{-4} between the points at $\tau = 0$ and $\tau = \tau_{max}$. A similar change of 3.8×10^{-4} occurs in the case of $v_B = 6000$ kms^{-1}. S_s in figure 3 correspondingly change by factors 8.9×10^{-5} and 7.9×10^{-6} at $\tau = 0$. The changes in the source functions

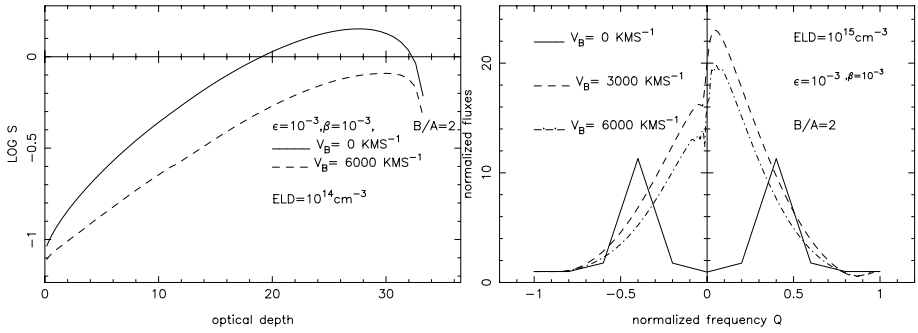

Figure 14. Source functions and the corresponding line profiles.

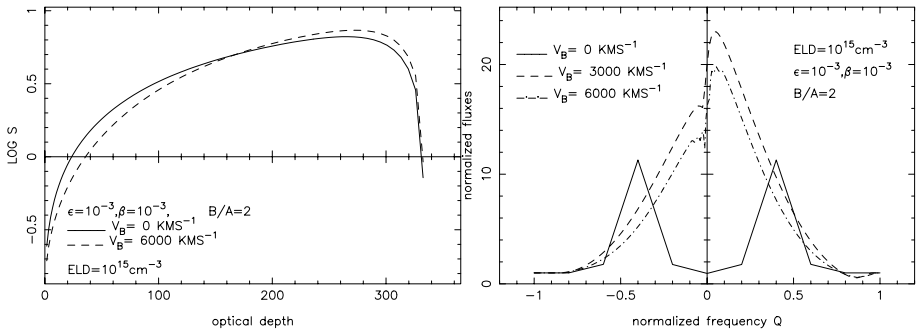

Figure 15. Source functions and the corresponding line profiles.

from those in the stationary media to those in the expanding media do not appear to be large as these are given in the logarithmic scale. The source functions in figures 4 and 5 for $B/A = 10$ and those in figures 6 and 7 have similar characteristics. The line profiles given in figure for $v_B = 0\ Km/s$ is a symmetric absorption profile. The profiles for $V_B = 3000$ kms^{-1} and at higher velocities , show P Cygni type characteristics with red emission and blue absorption with the centre of the line being shifted towards blue side of the centre of the line. This is due to the fact that the matter in the radially expanding atmosphere exactly opposite to the observer approaches towards the observer and contributes to the absorption shifting the centre towards blue side due to the Doppler effect. The radiation coming from the lobes of the atmosphere contributes to the emission in the line (for details, see Peraiah, 2002, Chap 8). This emission appears slightly in the red side of the centre of the line. The two line profiles for $V_B = 3000, 6000$ kms^{-1} show similar structure with the difference that the profiles for higher velocities show deeper absorption on the blue side. This is due to radiation being advected by the high velocity of the gas which will not contribute to the line fluxes. The profiles of the lines given in figure 3 ($ELD = 10^{15}\ cm^{-3}$) are similar to those given in figure 2 with the difference that the latter profiles are broader. This occurs because in the thicker medium more photons are scattered away from the line centre making it deeper and broader. The results in

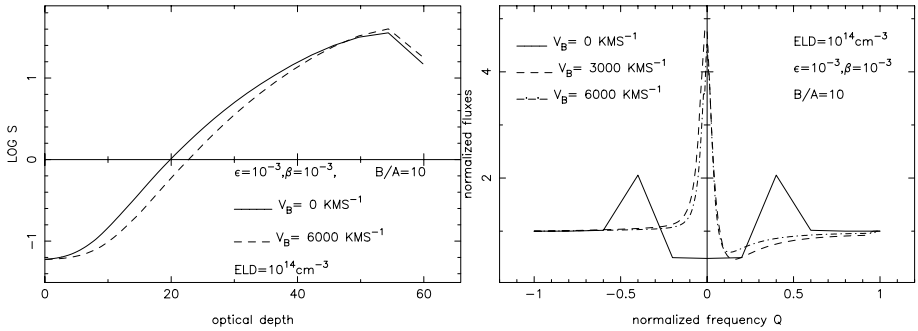

Figure 16. Source functions and the corresponding line profiles.

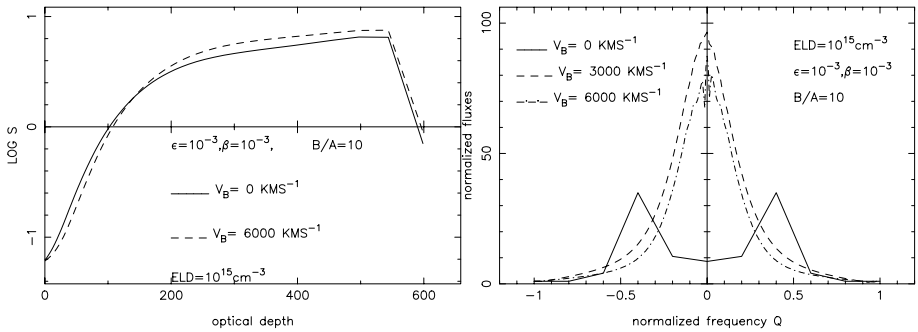

Figure 17. Source functions and the corresponding line profiles.

figures 6 and 7 are for $B/A = 100$. The emission at the centre is larger than those given in figures (2-5). In these two figures, the electron densities are 10^{14} and 10^{15} cm^{-3}. The source functions are considerably different and the profiles for $v_B > 0$ in the latter case are more broadened than those in the former case because of large optical depth which implies more scattering of photons away from the centre of the line. The normalised line flux ratios are almost the same in the two cases although the actual fluxes are different(these are not shown here). We presented the results of case(2)($\epsilon = 10^{-3}$ and $\beta = 0$) in figures (8-13). No incident radiation is given on either side of the atmosphere. Continuum emission comes through the Planck function ($B(T_e, x) = 1$). Figures 8 and 9 contain the source functions for $B/A = 2$ and $ELD = 10^{14}$ and $10^{15} cm^{-3}$, respectively. The source function reaches a maximum between $\tau = 0$ and $\tau = \tau_{max}$. The maximum does not occur at $\tau = \tau_{max}$ as in the case of atmospheres of case(1). The continuum contributes to the radiation field through the thermalised photons $\epsilon B(T, x)\tau$) and those scattered in the line. The source functions in the figures 10, 11, 12, and 13 show similar physical characteristics. The right handside of figures(8-13) show the line profiles corresponding to the source functions given in the respective figures. The profiles in static media show symmetric lines with double emission peaks and central absorption. The profiles given in figures 8 and 9 representing expanding media with $B/A = 2$ show central emission

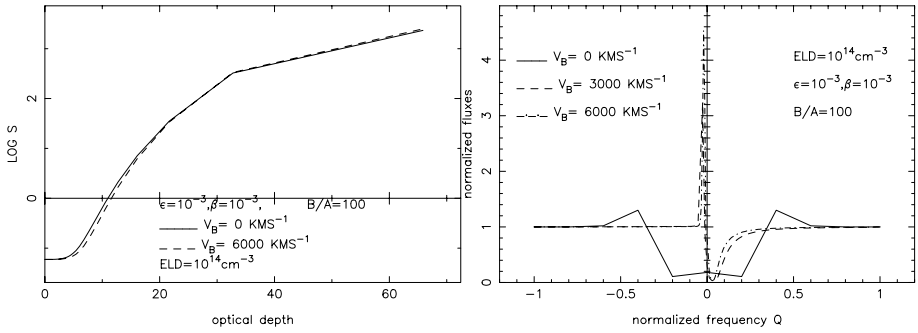

Figure 18. Source functions and the corresponding line profiles.

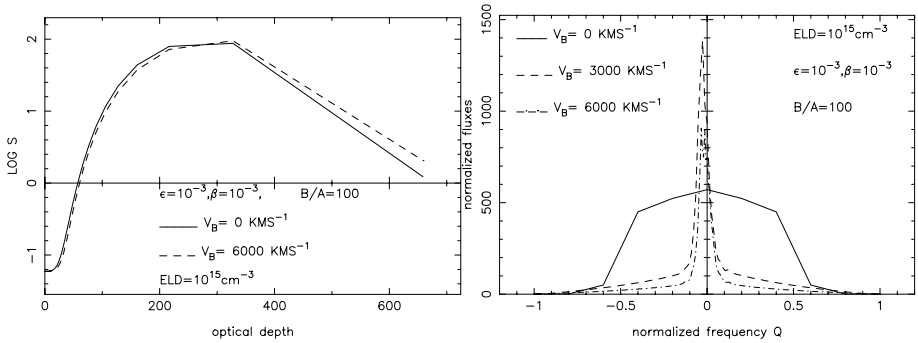

Figure 19. Source functions and the corresponding line profiles.

with no self absorption. The figure 10 for($B/A = 10$ and $ELD = 10^{14}$) show typical P Cygni profiles. When the gases expand, the emission peak on the red side of the centre gets shifted towards blue side or the centre of the line due to the Doppler effect. The central absorption core will shift towards the blue side and joins the emission wing and disappears. The emission peak on the blue side will shift to the continuum. Thus only emission peak appears. Results in figures 11, 12, 13 are similar in nature. Results of figures (14-19) represent the physics of the atmospheres of case(3) in which the radiation field gets contributions from both continuum and line. The results of this case are very similar to those of the atmospheres of case(2). The optical depth changes by a factor of 10 between the figures (14) and (15). In figure (14) the profile in static case is an emission line while the profile in figure (15) (the atmosphere is 10 times optically thick), the profile in static medium has two emission wings with a self absorption core. More photons are scattered away from the centre of the line in an optically thick medium. The profiles in the expanding media are sharp emission lines in the former case while in the latter case they are broad emission lines. Again the photons from continuum and those photons which are partly redistributed in the line contribute to this phenomema. The results in figures (16) to (19) can be explained the same way.

4. Conclusions

We studied the resonance line radiation field with partial frequency redistribution function in a rapidly expanding spherical medium by including the phenomena of aberration and advection. We considered different types of atmospheres with respect to their sizes, densities, physical characteristics and velocities of expansion. The emerging line profiles resemble the P Cygni type of profiles from a purely scattering atmospheres and those from emitting media will have central emission peaks or double emission peaks with self absorption.

5. Acknowledgements

I would like to thank Dr. B. A. Varghese for helpful suggestions.

References

Kor č ákov á, D. Kub ́bat, J., 2003,A and A, **401**,419.
Peraiah, A., 1987, APJ, **317**, 271.
Peraiah, A., 1991a, APJ, **371**, 673.
Peraiah, A., 1991b, APJ, **380**, 212.
Peraiah, A., 2002, An Introduction to Radiative Transfer:Methods and Applications in Astrophysics. Cambridge University Press, Cambridge, U.K.
Unno, W., 1952 Publ. Astron. Soc. Japan, **4**, 100.